# Spin-exchange relaxation-free magnetometry using elliptically polarized light

V. Shah* and M. V. Romalis
*Department of Physics, Princeton University, Princeton, New Jersey 08544, USA*
(Received 9 March 2009; published 24 July 2009)

Spin-exchange relaxation free alkali-metal magnetometers typically operate in the regime of high optical density, presenting challenges for simple and efficient optical pumping and detection. We describe a high-sensitivity Rb magnetometer using a single elliptically polarized off-resonant laser beam. Circular component of the light creates relatively uniform spin polarization while the linear component is used to measure optical rotation generated by the atoms. Modulation of the atomic spin direction with an oscillating magnetic field shifts the detected signal to high frequencies. Using a fiber-coupled distributed feedback laser, we achieve magnetic field sensitivity of 7 $\mathrm{fT}/\sqrt{\mathrm{Hz}}$ with a miniature $5\times5\times5$ mm Rb vapor cell.

DOI: 10.1103/PhysRevA.80.013416 PACS number(s): 32.80.Xx, 07.55.Ge, 42.65.−k

## I. INTRODUCTION

Alkali-metal magnetometers have recently achieved magnetic field sensitivity on the order of 1 $\mathrm{fT}/\sqrt{\mathrm{Hz}}$, previously possible at low frequencies only with superconducting quantum interference devices (SQUID) operating in liquid helium [1]. High sensitivity is obtained by operating at a high alkali-metal density of $10^{13}$–$10^{15}$ $\mathrm{cm}^{-3}$ in a spin-exchange relaxation-free (SERF) regime. In this regime, the rate of alkali-metal spin-exchange collisions is much greater than the Zeeman precession frequency, resulting in the reduction of the spin-exchange relaxation of the Zeeman coherences [2]. Magnetic field sensitivity in the femtotesla range opens a number of new applications previously accessible only for SQUID magnetometers [3,4]. Of particular interest is detection of biological magnetic fields from the heart or the brain [5,6], presently among the biggest area of SQUID use. In this application, tens to hundreds of SQUID sensors are placed around the subject to create a spatial map of the magnetic field. Detection and mapping of brain magnetic fields have been demonstrated with a SERF magnetometer using a large vapor cell and a multichannel photodetector [7]. However, the flexibility of magnetic field mapping would be greatly improved if one could instead use a collection of simple, compact, and self-contained atomic magnetometers while still maintaining high magnetic field sensitivity.

Here we describe such a compact, fiber-coupled atomic magnetometer. Our approach combines several novel features necessary for achieving high magnetic field sensitivity in a small detection volume. The magnetometer operates in the regime of high optical depth of several hundred on resonance, which presents challenges for efficient optical pumping and detection. In the conventional configuration [8], a circularly polarized pump beam is tuned to the center of the $D_1$ resonance to spin polarize the atoms and a linearly polarized probe beam is tuned off-resonance to measure the optical rotation induced by the atoms. The pump beam can propagate through the optically thick vapor only by pumping most of the atoms into the "dark" stretched state. However, this requires very high pumping rate which reduces sensitivity of the magnetometer by causing excessive power broadening of the magnetic resonance. The spin polarization at optimal pump power that maximizes the sensitivity is 50%. By detuning the pump laser off-resonance so that the optical depth is less than 1, it is possible to maintain the polarization of the alkali-metal vapor closer to the optimum value. For a pressure-broadened optical resonance, the efficiency of optical pumping can be maintained when the laser is detuned away from the resonance by increasing its intensity.

Detection of spin polarization is still performed using polarization rotation of the light, which is generally the most efficient "quantum nondemolition" technique of spin interrogation. It is also largely immune from laser intensity noise. The simplest method of light polarimetry involves a polarizing beam-splitter cube at 45° to the initial polarization and two photodetectors with balanced outputs. However, low-frequency sensitivity of this technique is usually degraded due to motion of the laser beam. Better performance at low frequency can be achieved if the polarization of the light is modulated, using, for example, a separate Faraday modulator [8]. However, this would not be practical in a compact, self-contained magnetometer. Therefore we use alkali-metal atoms themselves to modulate the polarization of the light. The direction of the atomic spin polarization is modulated by a large angle using an oscillating magnetic field, which in turn creates a large modulation of the light polarization. The signal proportional to the dc magnetic field is measured at the modulation frequency. We discuss the requirements for the choice of the modulation frequency so the vapor remains in the SERF regime. For sufficiently high alkali-metal density, the modulation frequency of several kHz can be used without significant loss in sensitivity, largely eliminating low-frequency noise associated with beam motion.

To reduce the overall complexity of the magnetometer, we use a single elliptically polarized laser beam for both pumping and probing. This reduces the efficiency of optical pumping by $\sqrt{2}$ and also reduces the optical rotation signal by $\sqrt{2}$. The light from a distributed feedback (DFB) laser is send to the sensor through a multimode optical fiber. Photodetectors are incorporated into the magnetometer. Off-resonant partially circularly polarized light causes a significant light shift and we discuss methods to mitigate its effects. We demonstrate magnetic field sensitivity of 7 $\mathrm{fT}/\sqrt{\mathrm{Hz}}$, limited by

*vishal.k.shah@gmail.com

 ©2009 The American Physical Society

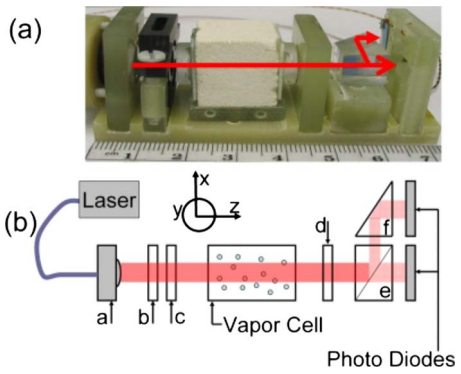


FIG. 1. (Color online) (a) Assembled magnetometer sensor (side view). (b) A schematic of magnetometer arrangement (top view). a is a fiber holder and a collimator, b is a linear polarizer, c is a quarter waveplate, d is a focusing lens and a half-wave plate combination, e is polarizing beam splitter, and f is a prism. The angle between the polarizer axis and the fast axis of the quarter wave is equal to $\pi/8$ and the angle between the polarizer axis and the half-wave plate axis is equal to $\pi/4$.

Johnson noise in the magnetic shields. The measurements are performed in a vapor cell with dimensions of $5\times5\times5$ mm. A fully integrated magnetometer physics package with a volume of 1 $cm^3$ roughly represents an optimal magnetometer size for noninvasive measurements on human subjects since magnetic field sources of interest are typically submerged several centimeters below the skin.

Earlier work on simplifying the operation of SERF magnetometers using spin modulation has been presented in [9,10]. In [9], a magnetic field modulation technique was used to shift the measured signal to higher frequencies. However, the relationship between the modulation frequency and the requirement for operation in the SERF regime was not discussed and separate pump and probe beams were used. In [10], a single circularly polarized laser beam tuned to resonance was used for both pumping and probing the vapor. The optical density of the alkali-metal vapor was restricted to be on the order of unity to avoid excessive absorption of the laser beam. The noise in the detection of the optical transmission was dominated by laser intensity noise. The magnetic field sensitivity demonstrated here is about 1 order of magnitude greater than in [9,10].

In Sec. II, we discuss the theory of atomic magnetometry using elliptically polarized light and magnetic field modulation in the SERF regime. In Sec. III, we describe the experimental implementation of the magnetometer and present comparison to theory and measurements of the magnetic field sensitivity.

## II. THEORY

We consider propagation of the light in an optical system shown in Fig. 1, representing the experimental arrangement used in this work. The light from a multimode fiber passes through a plate linear polarizer and a quarter-waveplate with its optic axis oriented at an angle $\theta$ relative to the linear polarizer. The propagation of the light through the Rb atomic vapor is conveniently analyzed in the circular polarization basis

$$\mathbf{E} = E_0[Ae^{ik_r z}\hat{\mathbf{R}} + Be^{ik_l z}\hat{\mathbf{L}}]e^{-2\pi i\nu t}, \tag{1}$$

where $\hat{\mathbf{R}}=(\hat{\mathbf{x}}-i\hat{\mathbf{y}})/\sqrt{2}$ and $\hat{\mathbf{L}}=(\hat{\mathbf{x}}+i\hat{\mathbf{y}})/\sqrt{2}$ are the right and left circular basis vectors and $\nu$ is the laser frequency. After the combination of linear polarizer and quarter-wave plate, $A=(\cos\theta+\sin\theta)/\sqrt{2}$ and $B=(\cos\theta-\sin\theta)/\sqrt{2}$. In the atomic vapor, the two circular components of the light experience different indices of refraction $k_r=2\pi\nu n_r/c$ and $k_l=2\pi\nu n_l/c$, which have both real and imaginary components to account for light retardation and absorption, $n_r=n_r^r+in_r^i$ and $n_l=n_l^r+in_l^i$. Polarization of the light after the vapor cell is analyzed using a polarizing beamsplitter oriented at an angle $\alpha$ relative to the optic axis of the waveplate and measured with a pair of photodetectors. The sum $\mathcal{S}$ and difference $\mathcal{D}$ of the photodetector signals are given by

$$\mathcal{D} = E_0^2 e^{-d(n_l^i+n_r^i)}\cos[2\alpha + d(n_l^r - n_r^r)]\cos 2\theta, \tag{2}$$

$$\mathcal{S} = \frac{E_0^2}{2}[(1+\sin 2\theta)e^{-2dn_r^i} + (1-\sin 2\theta)e^{-2dn_l^i}], \tag{3}$$

where $d=2\pi\nu l/c$ and $l$ is the length of the cell.

We consider here optical pumping on the $D_1$ line in an alkali-metal vapor in the presence of high buffer gas pressure. Therefore, the absorption profile is given by a pressure-broadened Lorentzian and the interaction (both absorption and dispersion) between atoms and photons is proportional to $(1-\mathbf{s}\cdot\mathbf{P})$, where $\mathbf{s}$ is the photon spin $\mathbf{s}=i\mathbf{E}\times\mathbf{E}^*/E_0^2$ and $\mathbf{P}=\langle\mathbf{S}\rangle/S$ is the electron-spin polarization [11,12]. Hence the indices of refraction are given by

$$n_r = 1 + \kappa(1+P_z)L(\nu)/\nu, \tag{4}$$

$$n_l = 1 + \kappa(1-P_z)L(\nu)/\nu, \tag{5}$$

where $L(\nu)=1/(\nu_0-\nu-i\Delta\nu/2)$ is a complex Lorentzian profile with a full width at half maximum (FWHM) $\Delta\nu$ centered at $\nu_0$. Here, $\kappa=nr_ec^2f/4\pi$, where $n$ is the alkali-metal density, $r_e$ is the classical electron radius, and $f\simeq1/3$ is the oscillator strength for the $D_1$ transition. For $\alpha=\pi/4$, we get for the photodiode difference signal $\mathcal{D}$,

$$\mathcal{D} = E_0^2 e^{-\sigma nl}\sin\phi\cos 2\theta, \tag{6}$$

where the absorption cross section $\sigma=cr_ef\,\mathrm{Im}[L(\nu)]$ and the optical rotation angle $\phi=cr_efnlP_z\,\mathrm{Re}[L(\nu)]$. The laser frequency $\nu$ is detuned off-resonance to generate a finite optical rotation angle $\phi$ proportional to the spin polarization $P_z$. With large detuning, we also have $\sigma nl\lesssim1$ to avoid significant light absorption in an optically dense alkali-metal vapor. Note that in the presence of spin polarization $P_z$, the light will become more circularly polarized after propagating through the vapor, but this affects only the sum of the intensities $\mathcal{S}$, not their difference $\mathcal{D}$.

To calculate the spin polarization of the alkali-metal atoms, we use Bloch equations that are valid in the SERF regime where the density matrix assumes a spin temperature distribution [13,14]

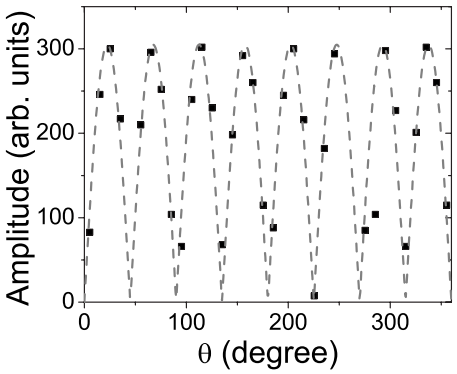


FIG. 2. (Dots) Experimental data showing amplitude of the zero-field resonance as a function of the angle between the polarizer and the quarter waveplate $\theta$. The measurements were made using low light intensities such that the rotation angle $\phi \ll \pi/4$. (Dash) Numerical fit to the data using a functional form of $|\sin(4\theta)|$ expected for the resonance amplitude in the low-polarization limit.

$$\frac{d\mathbf{P}}{dt} = D\nabla^2\mathbf{P} + \frac{1}{Q(P)}\left(\gamma\mathbf{P}\times\mathbf{B} + R(\mathbf{s}-\mathbf{P}) - \frac{\mathbf{P}}{T_2}\right), \quad (7)$$

where $D$ is the diffusion constant, $\mathbf{B}$ is the external magnetic field, $\gamma = 2\pi g_s \mu_B/\hbar = 2\pi \times 2.8 \times 10^{10}$ Hz/T is the electron gyromagnetic ratio, and $Q(P)$ is the nuclear slowing down factor that depends on the spin polarization [14]. $Q(P)=6$ for $^{87}$Rb in the low-polarization limit. $T_2$ is the transverse spin-relaxation time in the absence of the light, dominated by spin-destruction collisions with alkali-metal and buffer gas atoms. One can also approximately take into account the effects of spin relaxation on cell walls by additing the decay rate of the fundamental diffusion mode. $R$ is the optical pumping rate for an unpolarized atom, $R=\sigma\Phi$, where $\Phi = cE_0^2/(8\pi h\nu)$ is the photon flux. The photon spin $\mathbf{s} = -\sin 2\theta\hat{\mathbf{z}}$, ignoring changes in the polarization of the light due to propagation in the atomic vapor. First, consider a steady-state solution to Eq. (7) for the case when $B_y$ and $B_z$ are equal to zero. We get for $P_z$,

$$P_z = \frac{sR\tau}{\gamma^2 B_x^2 \tau^2 + 1}, \quad (8)$$

which is a zero-field Lorenztian resonance as a function of $B_x$ with a half width at half maximum (HWHM) $\Delta B_x = 1/\gamma\tau$, where $\tau = (R + 1/T_2)^{-1}$ is the atomic spin coherence time. If the optical rotation angle $\phi$ is small, then the height of the resonance measured in the photodiode difference signal $\mathcal{D}$ changes with the waveplate angle $\theta$ as $|\sin 4\theta|$. The experimentally measured resonance amplitude in the limit of low pumping rate and small spin polarization is shown in Fig. 2 as a function of $\theta$, confirming this behavior. The waveplate angle $\theta = \pi/8$ gives an optimal combination of optical pumping and probing with a single beam, reducing each by a factor of $\sqrt{2}$. It is also possible to achieve conditions when $\phi > \pi/2$, which results in a more complicated signal shape. The central feature of that shape near $B_x = 0$ becomes narrower, increasing magnetometer sensitivity.

One negative effect of optical pumping using off-resonant elliptically polarized light is that it generates significant light shift [15]. The light shift can be viewed as a fictitious magnetic field along the direction of light propagation whose magnitude is given by [11]

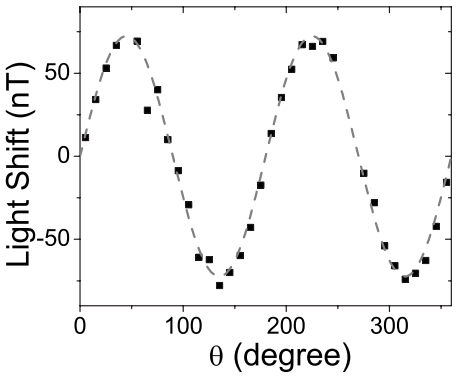


FIG. 3. (Dots) Experimentally observed light shift as a function $\theta$ under typical operating conditions. The light shift was measured by monitoring the strength of magnetic field in the $z$ direction required to minimize the zero-field resonance linewidth. (Dash) A fit to the experimental data using the functional form of the photon spin $s = \sin(2\theta)$. The absolute value of the light shift is consistent with Eq. (9) within a factor of 2 due to uncertainty in the incident light intensity.

$$\mathbf{B}_{LS} = scr_e f\Phi \ \mathrm{Re}[L(\nu)]/\gamma\hat{\mathbf{z}}. \quad (9)$$

It can be seen by finding a steady-state solution to Eq. (7) with a nonzero $B_z$ that the light shift will produce a broadening of the magnetic field resonance as a function of $B_x$. The light shift can be compensated by applying an equal and opposite real magnetic field in the $\hat{\mathbf{z}}$ direction. However, in practice, spatial inhomogeneity of light intensity due to transverse laser beam profile and absorption in the cell produces gradients of $B_{LS}$ that are difficult to compensate externally and results in residual broadening of the magnetic resonance. To reduce the effects of light-shift inhomogeneity, we expanded the Gaussian laser beam to a size larger than the cell and used only the relatively uniform central part of it. In Fig. 3, we show the average value of the light shift as a function $\theta$, measured by finding a value of external $B_z$ field that gives the narrowest resonance. The behavior of the light shift as a function of $\theta$ is consistent the expected $\sin(2\theta)$ dependence of the photon spin. It is possible to eliminate the effects of the light shift by periodically switching the frequency of the laser light to either side of the resonance on a time scale faster than the atomic spin coherence time. This would also introduce a high-frequency modulation into the measured rotation signal.

To use the zero-field magnetic resonance for sensitive measurement of $B_x$ field, we need to generate a dispersion signal with a steep slope centered around $B_x = 0$ [16,17]. We use a magnetic field modulation $B_x^{tot} = B_x + B_{\mathrm{mod}} \cos \omega t$ which also shifts detected signal to a higher frequency $\omega$ without the need for an external Faraday modulator or similar techniques. To determine the optimal modulation parameters, we consider the case when $\omega \gg (R + 1/T_2)$, going beyond steady-state solution of Eq. (7). The solution of the Bloch equations

in this regime has been obtained in [16]. In particular, the component of $P_z$ at the modulation frequency $\omega$ is given by

$$P_z(\omega) = \frac{2sR\gamma B_x \tau^2 \sin \omega t}{\gamma^2 B_x^2 \tau^2 + 1} J_0\left(\frac{\gamma B_{\mathrm{mod}}}{Q(P)\omega}\right) J_1\left(\frac{\gamma B_{\mathrm{mod}}}{Q(P)\omega}\right), \tag{10}$$

where $J_0$ and $J_1$ are Bessel functions of the first kind. This gives a dispersion signal as a function of $B_x$ with a maximum slope obtained when the modulation index $m = \gamma B_{\mathrm{mod}}/Q(P)\omega = 1.08$ and $R = 1/T_2 = 1/2\tau$.

It is generally advantageous to increase the modulation frequency while simultaneously increasing the modulation amplitude $B_{\mathrm{mod}}$ to move detected signal frequency further from technical noise sources at lower frequencies such as polarimetry noise arising from vibrations and thermal air convection and low-frequency noise in detection electronics. However when $B_{\mathrm{mod}}$ is sufficiently large, relaxation due to spin-exchange collisions begins to increase. In the regime when the spin-exchange rate $R_{se} \gg \gamma B_x^{tot}$ and the spin polarization is relatively low, the additional transverse spin relaxation due to spin-exchange collisions is given by [18]

$$\frac{1}{T_2^{se}(B_x)} = \frac{5}{18}\frac{\gamma^2 (B_x^{tot})^2}{R_{se}}, \tag{11}$$

for an alkali metal with $I = 3/2$, such as $^{87}$Rb. Since the frequency of $B_x$ modulation is much larger than the relaxation rate, we can calculate the average relaxation rate over one modulation cycle

$$\left\langle \frac{1}{T_2^{se}} \right\rangle = \frac{\omega}{2\pi}\int_0^{2\pi/\omega} \frac{1}{T_2^{se}(B_x)} dt = \frac{5}{36}\frac{\gamma^2 B_{\mathrm{mod}}^2}{R_{se}}, \tag{12}$$

assuming that $B_x$ is much smaller than $B_{\mathrm{mod}}$. In Eq. (10), the spin coherence time $\tau$ then becomes $\tau = (R + 1/T_2 + \langle 1/T_2^{se} \rangle)^{-1}$. The condition for maximum modulation frequency that can be used without loss of sensitivity is set by $\langle 1/T_2^{se} \rangle \lesssim R + 1/T_2$. This gives a modulation frequency $\omega \sim \sqrt{R_{se}/5T_2}$, which is much larger than $1/T_2$ in the SERF regime. For a given modulation frequency, one can find the optimal modulation amplitude from Eq. (10) taking into account changes in $\tau$ due to spin-exchange relaxation.

We find that for our experimental conditions, the optical rotation angle $\phi \propto P_z$ is often larger than $\pi/2$. In that case the photodetector difference signal $\mathcal{D} \propto \sin \phi$ is not a monotonic function of $P_z$. The modulation index $m$ can be adjusted to maximize the first harmonic signal in $\mathcal{D}$. The slope of the dispersion signal as a function of $B_z$ is maximized at a smaller value of $m$ and continues to increase with atomic path length $nl$. We find that in our experimental conditions, the optimal value of the modulation index $m$ is 0.5–0.8.

## III. EXPERIMENTAL SETUP AND RESULTS

A schematic of the experimental setup is shown in Fig. 1(b). The light from a 795 nm DFB laser tuned close to $^{87}$Rb $D_1$ transition was coupled into a multimode optical fiber and was delivered to the magnetometer setup. At the entrance of the magnetometer package, a planoconvex lens was used to collimate the light after which a sheet linear polarizer was used to define the polarization axis of the incoming light. Elliptically polarized light was created using either a $\lambda/4$ waveplate oriented at $\theta = \pi/8$ or a $\lambda/8$ waveplate oriented at $\theta = \pi/4$ relative to the linear polarizer. The beam passed through a cubical atomic vapor cell containing enriched $^{87}$Rb and approximately 300 Torr helium and 100 Torr $N_2$ buffer gases. The inner volume of the vapor cell was 0.09 cm$^3$. It was housed in a boron-nitride oven that was electrically heated using a high resistance titanium wire. The operating temperature of the cell was approximately 200 °C. The boron-nitride oven was enclosed in a low thermal-conductivity ceramic to reduce heat loss due to convection. To prevent magnetic fields generated by the electrical heaters from interfering with magnetic field measurements, the heater current was turned on and off with a duty cycle of 50% at a frequency of 0.02–0.2 Hz. The measurements were made while the heating current was off. In other experiments, we have successfully used ac currents at 20–100 KHz to heat the cell continuously without affecting magnetic field measurements [19]. The light transmitted through the vapor cell passed through a half-wave plate and was analyzed using a polarizing beam splitter and a pair of silicon photodiodes. The half-wave plate was rotated to balance the intensity in the two detectors in the absence of optical rotation from atoms.

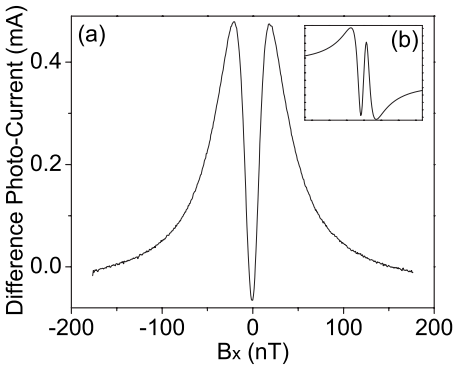


FIG. 4. (a) A typical zero-field resonance seen as a function of transverse magnetic field $B_x$ when $B_y$ and effective $B_z$ magnetic fields are zeroed. The resonance has multiple peaks due to optical rotation angles greater than $\pi/4$. We estimate that roughly 40% contribution to the linewidth comes from residual light shifts. (b) Lock-in amplifier dispersion signal. The $x$ axis spans from –200 to 200 nT. The $y$ axis is in arbitrary units. A 2 kHz sinusoidal magnetic modulation of 200 $\mathrm{nT}_{peak}$ amplitude was applied to $B_x$ to generate the signal.

Figure 4 shows a narrow zero-field SERF resonance signal obtained by monitoring photodiode difference signal as a function of $B_x$ field. Note that the rotation signal "turns over" because it exceeds $\pi/4$. The $B_y$ field and the sum of $B_z$ and $B_{LS}$ were zeroed by minimizing the linewidth of the resonance. The average light intensity at the entrance of the cell was about 40 mW/cm$^2$ and the rubidium density was $8 \times 10^{14}$/cm$^3$. The laser was detuned from the resonance by about 45 GHz where the optical density $\sigma nl$ was close to unity while the optical depth on resonance was 200. The relaxation rate $1/T_2$ due to a sum of Rb-Rb spin destruction,

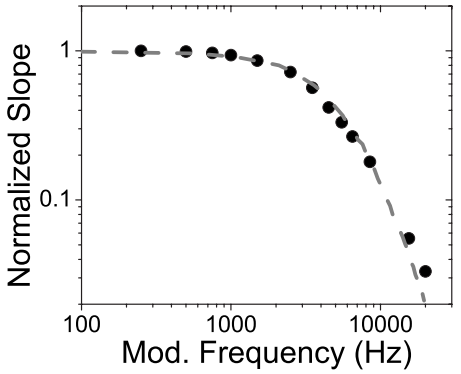


FIG. 5. (Dots) Normalized lock-in amplifier signal slope around $B_x=0$ as a function of the modulation amplitude for a fixed ratio of modulation amplitude to frequency equal to 0.17 nT/Hz which corresponds to modulation index $m=0.8$. (Dash) Predictions for the slope based on Eq. (10).

Rb-buffer gas spin destruction, and wall collisions was $1/T_2=1200\ \mathrm{s}^{-1}$ and the optical pumping rate $R=880\ \mathrm{s}^{-1}$. The average light shift expressed in terms of a fictitious magnetic field $B_{LS}$ was about 35 nT.

To operate as a magnetometer, the zero-field resonance was converted to a steep dispersive line shape centered around $B_x=0$ using additional modulation of $B_x$ field. The output of a lock-in amplifier with a phase of 90° relative to the modulation is shown in the inset of Fig. 4. The shape of the signal is more complicated than a simple dispersion curve due to large optical rotations. The modulation index is adjusted to maximize the slope of the dispersion curve near $B_x=0$. In Fig. 5, we show the slope at the zero crossing as a function of the frequency and amplitude of the modulation field with the modulation index $m=\gamma B_{\mathrm{mod}}/Q(P)\omega=0.8$ held fixed. The slope does not change substantially for modulation frequencies up to 2 kHz, about 10 times larger than the bandwidth of the magnetometer, in agreement with predictions.

In Fig. 6, we show the noise spectrum of the magnetometer when operated in the neighborhood of $B_x=0$ with a modulation frequency of 2 kHz. Except for spikes at discrete frequencies, the spectrum of the magnetic field noise is limited by Johnson noise in magnetic shields [20]. Polarimetry noise in the absence of the effects of the atoms can be tested by turning off magnetic field modulation. It is slightly lower but still above photon shot noise. Increasing the modulation frequency to 5 kHz reduces polarimetry noise but also broadens magnetic resonance due to turn-on of the spin-exchange relaxation. Operating at even higher Rb density would avoid this problem.

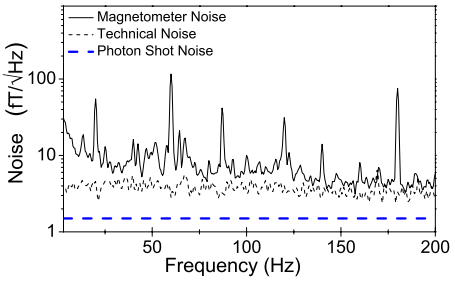


FIG. 6. (Color online) (Solid line) Spectral density of the magnetic field noise. The 3 dB bandwidth of the magnetometer was 150 Hz. (Dashed line) Polarimetry technical noise observed by switching off the modulation field used for lockin detection. (Thick dashed line) Calculated photon shot-noise-limited sensitivity of the magnetometer.

## IV. CONCLUSION

In conclusion, we have theoretically and experimentally examined a simple scheme for implementing SERF magnetometer using a single off-resonant elliptically polarized light beam. This scheme combines both simplicity and high performance to achieve femtotesla level sensitivity using a miniature vapor cell with an inner volume of 0.09 $\mathrm{cm}^3$. The complete magnetometer package consisting of optics, heated vapor cell, and a pair of photodetectors occupied 40 $\mathrm{cm}^3$ that we believe can be further reduced by over 1 order of magnitude in a relatively straightforward way. A compact sealed package would also likely improve low-frequency noise of the magnetometer. The laser light used here was coupled into the magnetometer using a multimode optical fiber which demonstrates the ability to operate an array of independent SERF sensors using a single high-power laser. Magnetic field modulation can either be applied by a common large coil to all sensors [7] or individually to each cell using small coils designed to produce a zero dipole and quadrupole magnetic moments at large distances. The sensitivity and size of the magnetometer make it ideally suited for magnetoencephalography [5] and other multichannel applications that can operate near zero total magnetic field.

## ACKNOWLEDGMENT

This work was supported by an ONR MURI grant.

[1] D. Budker and M. Romalis, Nat. Phys. **3**, 227 (2007).
[2] W. Happer and A. C. Tam, Phys. Rev. A **16**, 1877 (1977).
[3] R. L. Fagaly, Rev. Sci. Instrum. **77**, 101101 (2006).
[4] M. P. Ledbetter, I. M. Savukov, D. Budker, V. Shah, S. Knappe, J. Kitching, D. J. Michalak, S. Xu, and A. Pines, Proc. Natl. Acad. Sci. U.S.A. **105**, 2286 (2008).
[5] M. Hämäläinen, R. Hari, R. J. Ilmoniemi, J. Knuutila, and O. V. Lounasmaa, Rev. Mod. Phys. **65**, 413 (1993).
[6] C. D. Gratta, V. Pizzella, F. Tecchio, and G. L. Romani, Rep. Prog. Phys. **64**, 1759 (2001).
[7] H. Xia, A. B. Baranga, D. Hoffman, and M. V. Romalis, Appl. Phys. Lett. **89**, 211104 (2006).
[8] I. Kominis, T. Kornack, J. Allred, and M. Romalis, Nature (London) **422**, 596 (2003).
[9] Z. Li, T. Wakai, and T. G. Walker, Appl. Phys. Lett. **89**, 134105 (2006).

[10] V. Shah, S. Knappe, P. D. Schwindt, and J. Kitching, Nat. Photonics **1**, 649 (2007).
[11] S. Appelt, A. B. Baranga, A. R. Young, and W. Happer, Phys. Rev. A **59**, 2078 (1999).
[12] W. Happer, Rev. Mod. Phys. **44**, 169 (1972).
[13] J. C. Allred, R. N. Lyman, T. W. Kornack, and M. V. Romalis, Phys. Rev. Lett. **89**, 130801 (2002).
[14] M. P. Ledbetter, I. M. Savukov, V. M. Acosta, D. Budker, and M. V. Romalis, Phys. Rev. A **77**, 033408 (2008).
[15] W. Happer and B. S. Mathur, Phys. Rev. **163**, 12 (1967).
[16] C. Tannoudji, J. Dupont Roc, S. Haroche, and F. LaLoe, Rev. Phys. Appl. **5**, 95 (1970).
[17] R. Slocum and B. Marton, IEEE Trans. Magn. **9**, 221 (1973).
[18] I. M. Savukov and M. V. Romalis, Phys. Rev. A **71**, 023405 (2005).
[19] T. W. Kornack, S. J. Smullin, S. K. Lee, and M. V. Romalis, Appl. Phys. Lett. **90**, 223501 (2007).
[20] S. K. Lee and M. V. Romalis, J. Appl. Phys. **103**, 084904 (2008).